Research Article

Cancer Immunology Research

Depletion of Tumor-Associated Macrophages with a CSF-1R Kinase Inhibitor Enhances Antitumor Immunity and Survival Induced by DC Immunotherapy

Floris Dammeijer[1,2], Lysanne A. Lievense[1,2,3], Margaretha E. Kaijen-Lambers[1,2], Menno van Nimwegen[1], Koen Bezemer[1,2], Joost P. Hegmans[1,2], Thorbald van Hall[4], Rudi W. Hendriks[1], and Joachim G. Aerts[1,2,3]

Abstract

New immunotherapeutic strategies are needed to induce effective antitumor immunity in all cancer patients. Malignant mesothelioma is characterized by a poor prognosis and resistance to conventional therapies. Infiltration of tumor-associated macrophages (TAM) is prominent in mesothelioma and is linked to immune suppression, angiogenesis, and tumor aggressiveness. Therefore, TAM depletion could potentially reactivate antitumor immunity. We show that M-CSFR inhibition using the CSF-1R kinase inhibitor PLX3397 (pexidartinib) effectively reduced numbers of TAMs, circulating nonclassical monocytes, as well as amount of neoangiogenesis and ascites in mesothelioma mouse models, but did not improve survival. When combined with dendritic cell vaccination, survival was synergistically enhanced with a concomitant decrease in TAMs and an increase in $CD8^+$ T-cell numbers and functionality. Total as well as tumor antigen–specific $CD8^+$ T cells in tumor tissue of mice treated with combination therapy showed reduced surface expression of the programmed cell death protein-1 (PD-1), a phenomenon associated with T-cell exhaustion. Finally, mice treated with combination therapy were protected from tumor rechallenge and displayed superior T-cell memory responses. We report that decreasing local TAM-mediated immune suppression without immune activation does not improve survival. However, combination of TAM-mediated immune suppression with dendritic cell immunotherapy generates robust and durable antitumor immunity. These findings provide insights into the interaction between immunotherapy-induced antitumor T cells and TAMs and offer a therapeutic strategy for mesothelioma treatment. *Cancer Immunol Res; 5(7); 535–46. ©2017 AACR.*

Introduction

With the implementation of checkpoint inhibition therapy for several malignancies, immunotherapy has become an effective strategy for some patients in the treatment of advanced cancer (1). Although a subgroup of advanced disease stage patients benefits and shows prolonged overall survival to these therapies, the majority of patients do not respond or eventually relapse. Efforts have been made to characterize the mechanisms behind immunotherapy efficacy, leading to the distinction among inflamed, immune-sensitive tumors, and non-inflamed tumors associated with immunologic exclusion or ignorance (2–4). Blocking antibodies to the programmed cell death protein-1 (PD-1) appear to be most effective in patients whose tumors have a preexisting immune cell infiltrate, which can be enhanced by immunotherapy (5). The next breakthrough in cancer immunotherapy will be finding ways to sensitize non-inflamed and resistant-inflamed tumors to therapy, thereby increasing response rates and survival in advanced stage cancer patients (2, 3).

The dismal prognosis of malignant mesothelioma has not improved in the last decades despite implementation of conventional cancer treatment modalities (6). Malignant mesothelioma is often characterized by a prominent stromal component, dominated by macrophages (7). These tumor associated macrophages (TAM) often display an "alternatively activated" ("M2") immune inhibitory phenotype characterized by the production of interleukin 10 (IL10) and surface expression of CD206 and inhibitory molecules such as PD-L1 (8). Furthermore, TAMs have been shown to be critical regulators of angiogenesis and they are closely linked to local tumor outgrowth and pleural fluid-mediated immune suppression in malignant mesothelioma patients (9–11). Furthermore, a high M2-TAM to $CD8^+$ T-cell ratio correlates with a poor prognosis in malignant mesothelioma patients (9, 12).

TAMs are dependent on macrophage-colony stimulating factor (M-CSF) for their survival, proliferation, and recruitment towards

[1]Department of Pulmonary Medicine, Erasmus MC, Rotterdam, the Netherlands. [2]Erasmus MC Cancer Institute, Erasmus Medical Center, Rotterdam, the Netherlands. [3]Amphia Hospital, Breda, the Netherlands. [4]Department of Medical Oncology, Leiden University Medical Center, Leiden, the Netherlands.

Note: Supplementary data for this article are available at Cancer Immunology Research Online (http://cancerimmunolres.aacrjournals.org/).

R.W. Hendriks and J.G. Aerts share senior authorship of this article.

Corresponding Author: Joachim G. Aerts, Erasmus University Medical Center, PO Box 2040, Rotterdam, CA 3000, the Netherlands. Phone: 317-6595-3121; Fax: 311-0703-4856; E-mail: j.aerts@erasmusmc.nl

doi: 10.1158/2326-6066.CIR-16-0309

tumors (8, 13). In addition, M-CSF promotes an M2 phenotype (14). M-CSF in the tumor and circulation is correlated with poor survival in several solid tumor types (15). For these reasons, different approaches to inhibit the M-CSF/M-CSFR pathway have been designed in order to deplete TAMs (16, 17). These molecules can be subdivided into antibodies targeting M-CSF, the M-CSFR, and small-molecule tyrosine kinase (TK) inhibitors with variable specificities for related kinases downstream from the receptors c-kit and FLT3 (15). The advantages of TK inhibitors over antibody-mediated therapies include (i) their ability to affect both murine and human M-CSFR–signaling, improving translatability across species, (ii) inhibition of autocrine M-CSF/M-CSFR-signaling, and (iii) the absence of rebound monocytopoeiesis after cessation of therapy due to intact receptor-mediated internalization of M-CSF which is TK-independent (13). PLX3397 (pexidartinib) is a clinically tested inhibitor of M-CSF-receptor (M-CSFR) and c-kit tyrosine kinase. PLX3397 is safe and effective in reducing TAMs in several solid tumor types (17, 18). Whether PLX3397 is effective in depleting TAMs in mesothelioma, and possibly capable of restoring antitumor immunity in these tumors is currently unknown.

Therapies dependent on dendritic cells (DC) and T cells circumvent aberrant antigen presentation and the formation of ineffective immune responses in cancer, possibly explaining their efficacy over conventional tumor vaccines (19). We have previously demonstrated that vaccination is a safe and effective way to generate functional antitumor immunity and clinical responses in malignant mesothelioma patients (20, 21). We hypothesize that TAM-mediated immune suppression could limit DC-vaccination efficacy and that depletion of TAMs would improve response rates and response durability in malignant mesothelioma models.

Here, we show that PLX3397 is effective in depleting TAMs but that monotherapy does not improve survival in murine mesothelioma models. Combining M-CSFR inhibition with DC vaccination (DC therapy) to induce effective antitumor immune responses improved survival such that mice were protected from disease following tumor rechallenge. This therapeutic synergy may improve response rates and survival with immunotherapy.

Materials and Methods

Mesothelioma mouse models

Female 8–12-week-old BALB/c (H-2d) mice (Envigo) and CBA/J mice (Janvier) were housed under specific pathogen-free conditions at the animal care facility of the Erasmus MC, Rotterdam. Experiments were approved by the local Ethical Committee for Animal Welfare and complied with the Guidelines for the Welfare of Animals in Experimental Neoplasia by the United Kingdom Coordinating Committee on Cancer Research (UKCCCR) and by the Code of Practice of the Dutch Veterinarian Inspection. The AB1 cell and AC29 mesothelioma cell lines were kindly provided by Professor Bruce W.S. Robinson (Queen Elizabeth II Medical Centre, Nedlands, Australia). These cell lines were derived from tumors induced by crocidolite asbestos injected i.p. into CBA/J and BALB/c mice (22). Both cell lines were obtained in the years 2003–2005, aliquoted and stored at −190°C.

Tumor cells were cultured from early passages (max. 5 passages following cell line acquisition) in RPMI 1640 medium containing 25 mmol/L HEPES, Glutamax, 50 g/mL gentamicin, and 5% (v/v) fetal bovine serum (FBS) (all obtained from Gibco) in a humidified atmosphere and at 5% CO_2, in air. For culture, either culture flasks or CellSTACKs (Corning Life Sciences) were used to reach appropriate tumor cell frequencies for injection. AB1 and AC29 cells were passaged once or twice a week to a new flask by treatment with 0.05% trypsin, 0.53 mmol/L EDTA in phosphate buffered saline (PBS, all Gibco). At every 8–10 passages, cell lines were tested for mycoplasma contamination by PCR and remained negative. At the start of the experiment, CBA/J or BALB/c mice were i.p. injected with either 20×10^6 AC29 cells or 0.5×10^6 AB1 cells respectively, dissolved in PBS, or with PBS as control as was described previously (23). Mice were scored using the body condition score, killed if profoundly ill and scored as a death in survival analysis.

Tumor lysate production

AB1 cell line-derived tumor lysate was prepared as previously described (23). Briefly, cells were suspended in PBS and frozen in liquid nitrogen and disrupted by four cycles of freeze-thawing followed by sonication for 3×10 seconds with an amplitude of 10 μm, using a Soniprep 150 ultrasonic disintegrator equipped with a microtip (Sanyo Gallenkamp BV) on ice. Cell lysate was aliquoted and stored at −80°C.

Culture conditions of bone marrow-derived DC used for vaccination

DCs were generated following an adapted protocol (Lutz and colleagues 1999) as previously described (23). Bone-marrow derived cells seeded in 100-mm Petri dishes (day 0) and cultured in 10 mL DC Culture Medium [DC-CM]: RPMI 1640 containing glutamax-I (Gibco) supplemented with 5% (v/v) FBS, 50 mol/L mercaptoethanol (Sigma-Aldrich), 50 g/mL gentamicin (Invitrogen), and 20 ng/mL recombinant murine granulocyte macrophage-colony-stimulating factor (GM-CSF, kindly provided by Prof. B. Lambrecht, VIB Ghent, Belgium). Cells were cultured in a humidified atmosphere at 5% CO_2 in air. At day 3, 10 mL of fresh DC-CM was added. On day 6, 10 mL of each plate was replaced with 10 mL of fresh DC-CM. After 9 days of culture, AB1 cell lysate was added to the DC cultures, to the equivalent of three AB1 cell-equivalents per DC. After 8 hours, 10 g/mL CpG (ISS-ODN 1668, Invitrogen) was added to the culture to allow complete maturation while incubated overnight. The next day, DCs were harvested by and purified by Lympholyte-Mammal (Cedarlane) density gradient centrifugation, the interphase was washed three times in PBS and resuspended at a concentration of viable cells. The quality of the DC preparation was determined by cell counting, morphologic analysis, and cell surface marker expression by flow cytometry, as previously described (23).

DC-culture with PLX3397

Mature, lysate pulsed-DCs were generated as demonstrated above and cultured for 48 hours in GM-CSF DC-TCM and varying concentrations of PLX3397 (provided by Plexxikon Inc. as part of a material transfer agreement; ref. 17) or the vehicle (Dimethyl sulfoxide, DMSO, Sigma-Aldrich) in 6-well plates. PLX3397 was reconstituted in DMSO to reach a stock concentration of 20 mmol/L, which was then diluted to a concentration range of 0.1 to 10 μmol/L in DC-TCM. After

48 hours, cells were harvested from the 6-well plates and analyzed for viability and surface expression of immune markers using multicolor flow cytometry.

Treatment with tumor lysate-pulsed DCs and/or PLX3397

On day 0, BALB/c or CBA/J mice were inoculated intraperitoneally with AB1 or AC29 tumor cells, respectively. On day 10, mice were treated with either 2–3 $\times$ 10^6 DCs dissolved in 200 μL PBS, or PBS alone. This time point was determined to be most optimal in previous experiments (23). In specified cases, treatment with either DC therapy alone or in combination with PLX3397 commenced at day 15 to allow for enough tumor to be collected several days later and prepare a window to detect possible changes between mono- and combination-treated tumors. Also, depending on the treatment arm, mice were fed *ad libitum* PLX3397-containing chow or control chow of equal nutritional value and consistency until the end of the experiment or prior to rechallenge. The optimal dose to effectively deplete TAMs was determined by Plexxikon and has been further corroborated in different tumor models to be 290 mg PLX3397/kg chow (delivering daily doses of approximately 45 mg/kg; ref. 24). On day 15 post-tumor cell injection, prior and after rechallenge, blood was obtained via tail vein extraction. During the remainder of the follow-up period, mice were examined daily for evidence of illness caused by overt tumor growth.

Immunohistochemistry (IHC) on tumor material

Tumor biopsies were embedded in Tissue-Tek II optimum cutting temperature medium (Miles), snap-frozen, and stored at −80°C. Tissue sections (6 μm) were cut on a cryostat (Cryostar NX70, Thermo Fisher Scientific). Frozen sections were warmed to room temperature, fixed with acetone for 10 minutes and rinsed in PBS. Sections were incubated in peroxidase blocking solution (0.1% H2O2 and 0.1% sodium azide in PBS) for 30 minutes and rinsed with PBS. Slides were placed in a semi-automatic stainer (Sequenza) and incubated in 1:10 diluted normal Goat serum (CLB) for 10 minutes and subsequently for 60 minutes with the diluted primary Abs, followed by rinsing in PBS for 5 minutes and incubation for 30 minutes with diluted secondary Abs. Double-immunostaining was carried out using antibodies supplied in Supplementary Table S1. Binding of antibody was detected using alkaline phosphatase- (AP-) or peroxidase-conjugated goat anti-rat (Sigma-Aldrich) and Naphtol-AS-MX-phosphate (0.30 mg/mL; Sigma-Aldrich) + new fuchsine (160 mg/mL in 2 mol/L HCl; Chroma-Gesellschaft) or AEC [0.1 mol/L NaAc + 1% AEC stock (100 mg AEC in 10 mL DMF), Vectorlabs], respectively, were used as substrate. The specificity was checked using a protein concentration-matched non-relevant rat antibody and PBS. Finally, the sections were rinsed in distilled water and mounted in vecta mount (Vector). Slides were scanned using a Nanozoomer 2.0 HT (Hamamatsu).

Quantification of IHC images

Scanned IHC slides were viewed using NDP-viewing software (Hamamatsu) at 20× and 40× magnification and regions of interest were captured and imported into ImageJ software (NIH). Colors were separated, thresholds were installed to select for positive cells and these were depicted as percentage of total area. For each sample, 5 random areas (including tumor rim and center) at 20× magnification were selected, analyzed and averaged. CD8-positive cells were well demarcated and counted (average of 5 random tumor areas per sample) to be expressed as cells/mm^2.

Preparation of single-cell suspensions from tissues

Single-cell suspensions were generated from the spleens, blood, and tumors of mice from each group. All tissues were either weighed in a microbalance in case of tumors and spleens, or volume determined for blood. Briefly, spleens were aseptically removed and mechanically dispersed over 100-μm nylon mesh cell strainer (BD Biosciences) followed by erythrocyte lysis using osmotic lysis buffer (8.3% NH_4Cl, 1% $KHCO_3$, and 0.04% Na_2EDTA in Milli-Q). Blood was collected in EDTA tubes (Microvette CB300, Sarstedt) and subsequently lysed. Tumors were collected and dissociated using a validated tumor dissociation system (Miltenyi Biotec). Cell suspensions were filtered through a 100-μm nylon mesh cell strainer (BD Biosciences) and counted in trypane blue with a hemocytometer using the Burker–Turk method.

Flow cytometry

For measurements of cytokine production in lymphoid cells by flow cytometry, cells were restimulated for 4 hours at 37°C using PMA and ionomycin supplemented with GolgiStop (BD Biosciences). For assessing cytokine production by myeloid cells, cells were subjected to 4 hours incubation with Golgistop. For cell surface marker staining, cells were washed with FACS-wash (0.05% NaN_3, 2% BSA in PBS) and Fc II/III receptor blocking was performed using anti-mouse 2.4G2 antibody (1:300; kindly provided by L. Boon, Bioceros, Utrecht, the Netherlands). After the blocking procedure, antibodies (Supplementary Table S1) for cell surface staining were added into each sample and placed on ice for 30 minutes. Cells were washed in FACS-wash followed by a PBS wash, and then stained for viability using fixable LIVE/DEAD aqua cell stain (Thermo Fisher Scientific, 1:200). After two additional washes with FACS-wash, cells were either measured or in case of intracellular staining; fixated, permeabilized, and stained using Fix/Perm buffer (in case of nuclear protein staining, eBioscience) or 4% PFA and 0.5% saponin (in case of cytokine stainings, Sigma-Aldrich). Antibodies were stained for 30 minutes in case of the PFA/Saponin protocol and 60 minutes for the intranuclear staining protocol, on ice in the dark. A fixed number of counting beads (Polysciences Inc.) was added prior to data acquisition to determine the absolute amount of cells. Data were acquired using an LSR II flow cytometer (BD Biosciences) equipped with three lasers and FACSDiva software (BD Biosciences) and analyzed by FlowJo (Tree Star, Inc.) software V10.1.

In order to detect tumor-antigen specific $CD8^+$ T cells in the CBA/J model, dextramers specific for potentially dominant WT1 and Mesothelin epitopes were constructed. Peptides for WT1 and Mesothelin were selected based on freely available tools (IEDB Analysis Resource) predicting likelihood of processing, MHC-I (H2-Kk) binding affinity and immunogenicity of the chosen peptides. The peptide sequences for WT1 and Mesothelin selected were SENHTAPIL, and QEATLLHAV, respectively. Dextramers were labeled to APC or PE fluorochromes and ordered from Immudex. Dextramers were stained independently from one another following company instructions on cells pretreated in RPMI containing 50 nmol/L Dasatinib for 30 minutes at 37°C to limit TCR internalization. FMO and dextramer binding-$CD4^+$ T cells were used to determine background signal and set cutoff limits.

Microarray analysis of AB1 and AC29

Biotin-labeled cRNA derived from AB1 and AC29 ($n = 3$ samples) was hybridized to the Mouse Genome 430 2.0 Array according to the manufacturer's instructions (Affymetrix); data were analyzed with BRB-ArrayTools (version3.7.0, National Cancer Institute) using Affymetrix CEL files obtained from GCOS (Affymetrix To examine the quality of the various arrays, the R package affyQCreport for generating QC reports was run starting from the CEL files. All created plots indicated a high quality of samples and an overall comparability. Raw intensity values of all samples were normalized by RMA normalization (Robust Multichip Analysis; background correction and quantile normalization) using Partek version 6.4 (Partek Inc.). Genes involved in myeloid cell chemotaxis and survival, and expression of clinically relevant tumor antigens were manually selected and plotted for both AB1 and AC29 cell lines. The GEO accession number for this microarray is GSE97150.

Statistical analysis

Data are expressed as medians with interquartile range. Comparisons between groups were made using the Mann–Whitney *U* test for independent samples, or the Wilcoxon signed rank test in case of paired samples. When correlations were depicted, Spearman's rank correlation test was performed to test for statistical significance. A two-tailed value of $P < 0.05$ was considered statistically significant. Survival data were plotted as Kaplan–Meier survival curves, using the log-rank test to determine statistical significance. Data were analyzed using GraphPad Prism software (Graphpad, V5.01)

Results

DC therapy synergizes with M-CSFR inhibition in orthotopic mesothelioma mouse models

In the past, we have shown that applying DC therapy in syngeneic and orthotopic mesothelioma mouse models is effective for assessing antitumor T-cell responses and evaluating treatment efficacy (23, 25). The AB1 and AC29 mesothelioma cell lines are injected intraperitoneally (i.p.) in BALB/c and CBA/J mice, respectively. Compared with the BALB/c model, the CBA/J model has a more pronounced TAM-dependent phenotype (Supplementary Fig. S1A), which may be explained by the increased expression of M-CSF and CCL-2, being key TAM-homing and survival factors as determined by microarray (accession number: GSE97150, Supplementary Fig. S1B). In line with this M2-TAM–dominant phenotype, CBA/J mice injected with AC29 mesothelioma cells develop ascites, paralleling disease heterogeneity also seen in mesothelioma patients (22, 26, 27).

Here, we used the M-CSFR–inhibitor PLX3397 to target TAMs *in vivo*. To confirm that there was no direct effect of PLX3397 on the murine mesothelioma cell lines, we analyzed expression of M-CSFR and c-kit using flow cytometry and tissue microarray analysis. We found negligible levels of both molecules (Supplementary Fig. S1B). To exclude any direct effects of PLX3397 on maturated tumor-lysate pulsed DCs to be administered in the DC therapy protocol, we cultured these cells *in vitro* with increasing concentrations of PLX3397 or vehicle alone, then measured cell viability and expression of relevant surface markers by flow cytometry (Supplementary Fig. S2). As previously reported, GM-CSF–cultured cells are composed of heterogeneous populations of DCs and macrophages, which we also identified in our system (Supplementary Fig. S2; ref. 28). Effects of PLX3397 on DC viability or surface expression of MHC-II, CD86, PD-L1, M-CSFR, and c-kit were negligible (Supplementary Fig. S2A). This resistance of DCs to PLX3397 could be explained by the rapid downregulation of M-CSFR surface expression following maturation using unmethylated CpG (Supplementary Fig. S2B-S2C).

Mice were left untreated or were treated at day 10, after solid tumors had established, using three different regimens: (i) PLX3397 was administered in chow and continued for the duration of the experiment, (ii) DCs were injected i.p. as monotherapy, or (iii) mice were subjected to double therapy (Fig. 1A and B). PLX3397 monotherapy failed to improve survival in both mesothelioma tumor models (Fig. 1C and D). DC therapy prolonged survival only in the AC29 tumor model. Combination therapy, however, enhanced survival in both tumor models, indicating therapeutic synergy (Fig. 1C and D).

M-CSFR inhibition causes a decrease in $CD206^+F4/80^+$ TAM numbers, blood vessel density, and ascites

To assess whether PLX3397 was effective in depleting TAMs, we focused on the CBA/J mesothelioma model, because this is more TAM-dependent. IHC analysis showed a decrease in $F4/80^+$ TAMs, $CD31^+$ endothelial cells, and $CD206^+$ (M2) cells in PLX3397-treated mice compared with control mice (Fig. 2A–G). TAMs are crucial for tumor angiogenesis and concomitant ascites production in metastatic ovarian carcinoma (29). Indeed, we found a correlation between $CD31^+$ endothelial and TAM areas in these tumors and a decrease in ascites volume in the PLX3397-treated mice (Fig. 2D and E). Tumors of untreated mice contained a $CD8^+$ T-cell infiltrate which was not further enhanced following TAM depletion (Fig. 2H).

Taken together, these findings show that M-CSFR inhibition effectively reduced TAMs, neo-angiogenesis, and ascites in mesothelioma mouse models, but did not improve local $CD8^+$ T-cell infiltration.

Combination therapy increased $CD8^+$ T-effector cells and depleted nonclassical monocytes in blood

We next sought to investigate the potential mechanisms that lead to enhanced survival in DC therapy only and combination immunotherapy arms in the CBA/J model. To this end, we extracted blood 5 days after start of treatment and analyzed the circulating immune compartment using flow cytometry (Supplementary Fig. S3). DC therapy caused an increase in $CD8^+$ T-cell numbers with $CD4^+$ $Foxp3^+$ T-helper–cell numbers remaining unchanged, whereas proliferation, as determined by Ki-67 expression, was increased in both T-cell subsets (Fig. 3A–D; Supplementary Fig. S4A). Numbers of T-regulatory cells (Treg) were decreased following DC therapy, a decline amplified by the addition of PLX3397 treatment, resulting in an improved $CD8^+$ T-cell/Treg-ratio (Fig. 3C; Supplementary Fig. S4B). DC therapy, but not the addition of PLX339, increased the frequency of short-lived effector cells (SLEC), as determined by KLRG1 expression, from almost undetectable to approximately 20% of total $CD8^+$ T cells (Fig. 3E). In addition to proliferation, an increased proportion of $CD8^+$ T cells in the combination therapy–arm coexpressed CD4, which has previously been associated with increased $CD8^+$ T-cell effector functions (Fig. 3D and F; ref. 30, 31). These CD4/CD8 double-positive cells were also highest in proliferation in all treatment arms as demonstrated by increased proportions of Ki-67^+ cells (Supplementary Fig. S4C–S4D).

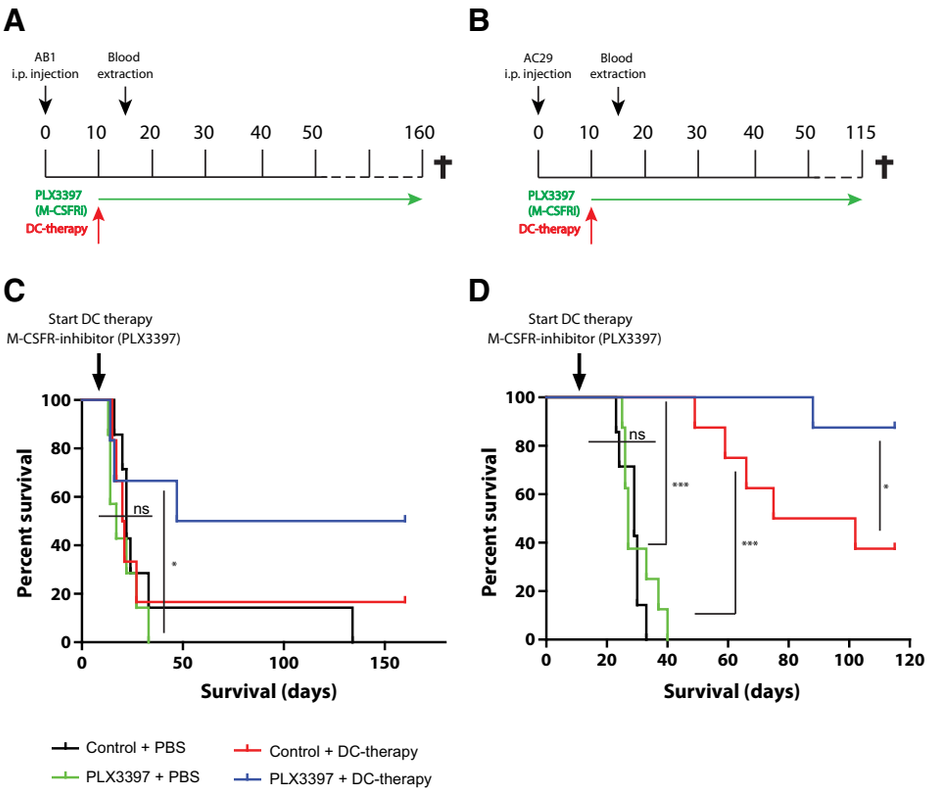

Figure 1.
Efficacy of DC therapy is synergistically enhanced by combination therapy with TAM depletion in mesothelioma mouse models. **A** and **B,** Wild-type, female BALB/c ($n = 6$/arm) and CBA/J ($n = 8$/arm) mice were i.p. injected with either 0.5×10^6 AB1 or 20×10^6 AC29 syngeneic tumor cells, respectively. Mice were then treated once on day 10 with either i.p. administration of PBS or mature, autologous tumor lysate loaded DCs. Concurrently, mice were started on control or PLX3397-containing chow until the end of the experiment or until rechallenge. Blood was extracted on $t = 15$ days and before and after rechallenge in case of CBA/J mice. Animals were monitored daily for the duration of 160 days and euthanized in case of severe illness. **C** and **D,** Kaplan–Meier curves of the survival experiments in CBA/J (AC29) and BALB/c (AB1) mesothelioma tumor models. Statistical significance was determined using the log-rank test with $P < 0.05$ being statistically significant. *, $P < 0.05$; **, $P < 0.01$; ***, $P < 0.001$; ns, not significant.

Whereas DC therapy primarily influenced lymphocyte dynamics and phenotype, PLX3397 therapy predominantly affected myeloid subsets (Fig. 4). Granulocyte and total monocyte numbers were increased by DC therapy but only granulocyte numbers were increased by PLX3397 as mono- or combination therapy (Fig. 4A and B). Monocytes can be subdivided into classical Ly6Chi- and nonclassical Ly6Clow monocytes with each subset having different functions and migration patterns in blood (32, 33). Dissecting monocyte subsets in our model revealed nearly complete depletion of nonclassical ($Ly6C^{low}$) monocytes in the PLX3397-treated arms (from ~40 to 5–10 cells/μL blood), whereas classical ($ly6C^{hi}$) monocytes numbers were slightly increased from ~50 to 75 cells/μL (Fig. 4C and D). Approximately 90% of nonclassical monocytes expressed PD-L1 in untreated conditions which was decreased to 20% to 40% of monocytes by M-CSFR-inhibition (Fig. 4F). Classical monocytes were rarely positive for PD-L1 (1%–5%), which was similar in DC therapy and combination therapy-treated mice (Fig. 4E).

Overall, the observed synergy between therapies was illustrated in the CBA/J model by an improved $CD8^+$ T-cell phenotype primarily in response to DC therapy, and a decrease in PD-$L1^+$ nonclassical monocytes due to PLX3397 treatment. Similar patterns in blood immune cell dynamics could be discerned in the AB1 tumor model; however, numbers of mice were limited at day 5 after start of treatment (Supplementary Fig. S5).

Tumors of mice treated with combination therapy had a favorable tumor microenvironment

To examine the tumor microenvironment (TME) for the effects of treatment and to relate these to changes in immune cell composition observed in spleen and blood, we sacrificed mice at day 15 in our CBA/J model. Five days after therapy began, we observed a similar tumor burden between the different treatment groups (Fig. 5A). TME immune composition at day 15, however, differed between treatment groups in line with interim analyses in blood and findings in end stage disease tumors of diseased mice (Supplementary Fig. S6A). Both $IL\text{-}10^+$ (M2) and $IL10^-$ (M1) TAMs were diminished by PLX3397 as monotherapy or in combination with DC therapy (Fig. 5B). We also further characterized peripheral blood nonclassical monocytes as being higher in IL10 and PD-L1 expression and lower in surface MHC-II expression, further establishing their immune suppressive phenotype (Supplementary Fig. S6B).

Confirming earlier results, the numbers of $CD8^+$ tumor-infiltrating lymphocytes (TIL) were not altered following PLX3397 monotherapy, and these TILs displayed an exhausted phenotype (34), defined as PD-1 positive, lymphocyte-activation gene 3 (LAG-3) positive, and interferonγ (IFNγ) negative (Fig. 5C). DC therapy, in contrast, enhanced the number of non-exhausted $CD8^+$ T cells in the tumor. This did not differ between DC therapy only and combination therapy-treated mice (Fig. 5C). To investigate whether this was a kinetics-related phenomenon, we treated tumor-bearing mice on day 15 and analyzed the tumor 8 days later to allow for proper T-cell infiltration. In addition, we sought to identify T-cell clones specific for the clinically meaningful tumor antigens Mesothelin and Wilms Tumor 1 (WT1) to assess whether $CD8^+$ T cells with these tumor specificities were enhanced by DC therapy and possibly enriched or improved in phenotype by coadministration of PLX3397. Both tumor antigens were highly expressed by the AC29 mesothelioma cell line

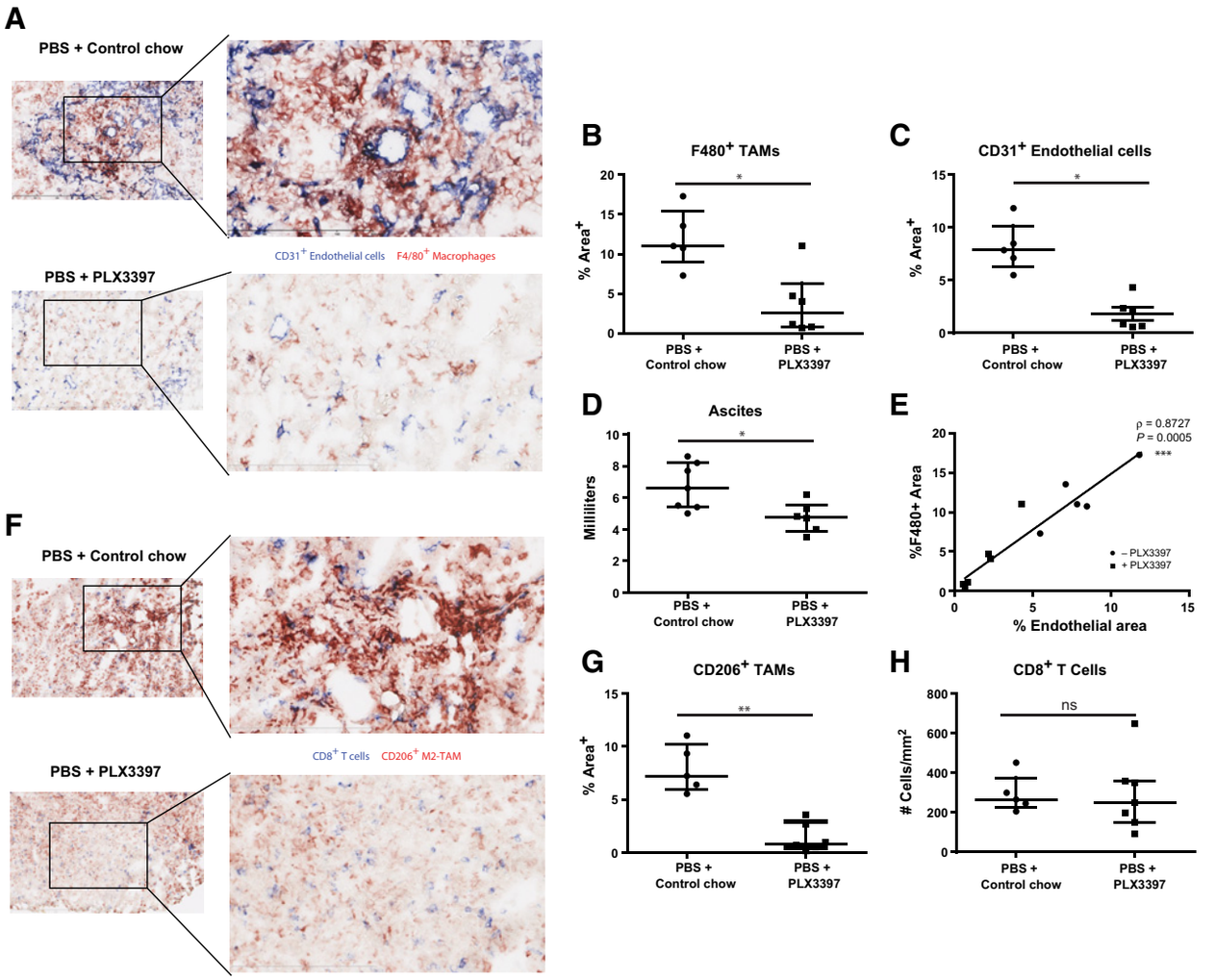

Figure 2.

TAM depletion causes a decrease in ascites production in CBA/j mice accompanied by a decrease in $CD206^+F4/80^+$ macrophages and blood vessel density. **A,** Tumors of untreated and PLX3397 only treated mice were extracted and tissue sections were double stained for TAMs, (F4/80, red) and endothelial cells (CD31, blue) using IHC. Tissues are displayed at a 20× magnification (error bar length is 400 μm) with a further close-up at 4048 magnification (error bar length is 200 μm). **B** and **C,** $F4/80^+$ TAMs and $CD31^+$ endothelial cells were quantified in both groups using ImageJ software on 5 independent tumor sections (including tumor center and rim) at 20× magnification and averaged to be expressed as percentage of total area. **D,** When mice were sacrificed at end stage disease, ascites was aspirated and the volume was measured and expressed as milliliters. **E,** TAM- and endothelial cell density was correlated in untreated (circles) and PLX3397-treated (squares) mice. **F,** Tissue sections were double stained for CD206-positivity (M2-TAM marker, red) and $CD8^+$ (cytotoxic T cells, blue) using IHC. **G,** $CD206^+$ positive cells were quantified similar to B–C and expressed as percentage of total area. **H,** $CD8^+$ T cells were counted (5 individual areas per tumor and averaged) and expressed as cells per cubic millimeter of tumor area (mm^2). All data are displayed as dot plots including the median and error bars indicating interquartile range. Statistical significance was determined using the Mann–Whitney *U* test with $P < 0.05$ being statistically significant. The Spearman's Rank Correlation coefficient (rho) was determined in case of Fig. 2E. *, $P < 0.05$; **, $P < 0.01$; ***, $P < 0.001$; ns, not significant; DC-Tx, DC therapy; TAM, tumor-associated macrophage.

(Supplementary Fig. S1B). T cells specific for these antigens were present in tumors from mice in all treatment groups, with an increase in WT1-specific but not Mesothelin-specific $CD8^+$ T cells in DC therapy-treated mice (Fig. 5D). There were prominent differences in $CD8^+$ T-cell phenotype in combination therapy-treated mice compared with those receiving DC therapy only, as determined by a higher proportion of PD-1–negative and –intermediate expressing cells (Supplementary Fig. S7). These cells are capable of eliciting potent antitumor functions (35–37). In line with this less-exhausted phenotype is the lower expression of coinhibitory molecules TIM3 and LAG3, and lower expression of CD8 indicative of enhanced activation (Supplementary Fig. S7B; ref. 38). Similar shifts in PD-1–expression were detected in both the Mesothelin- and WT1-specific T cells (Fig. 5E; Supplementary Fig. S7D).

In summary, we observed a PLX3397-dependent reduction in TAM frequency with a concurrent DC therapy dependent increase in tumor infiltrating $CD8^+$ T cells whose phenotype was improved upon TAM-depletion as shown by a decrease in proportion of PD-1-high $CD8^+$ T cells associated with T-cell exhaustion.

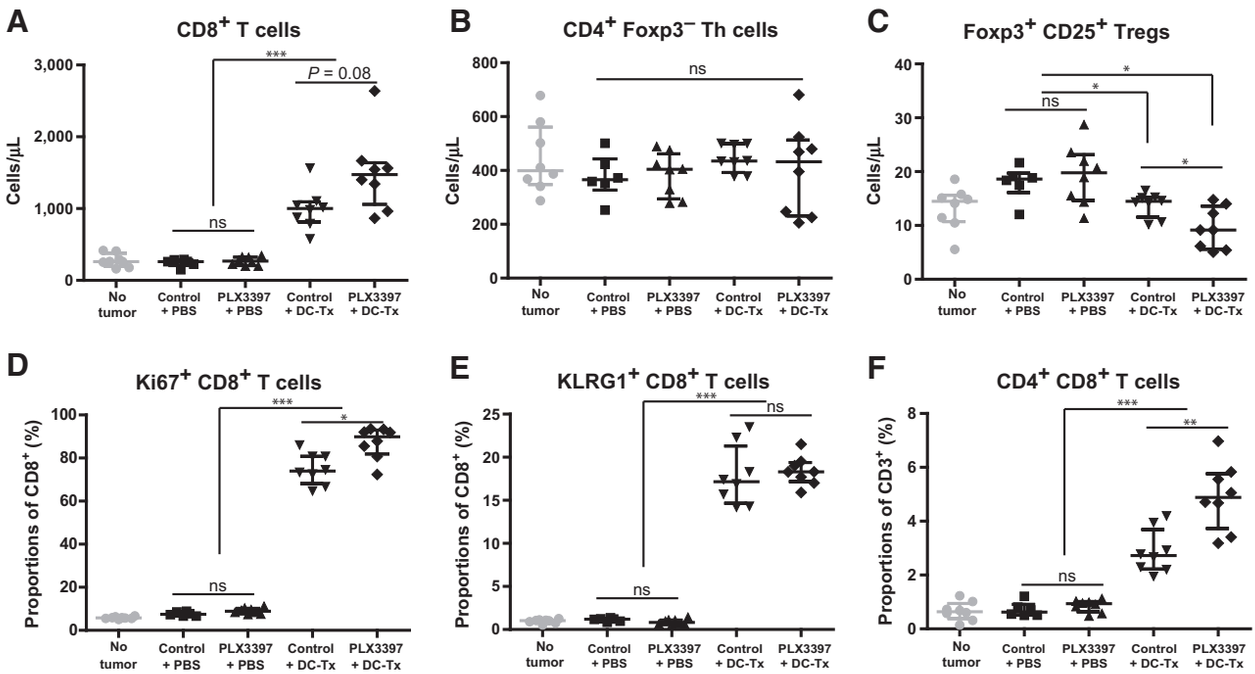

Figure 3.

$CD8^+$ T-cell proliferation and effector phenotype are further enhanced when combining TAM depletion with DC therapy whereas Tregs decrease in blood during therapy. **A–C,** Blood was extracted 5 days after start of treatment (day 15 after tumor cell injection) from all CBA/J mice ($n = 8$/group) and was analyzed by multicolor flow cytometry. Immune cell subsets were characterized as displayed in Supplementary Fig. S2A. **D–F,** $CD8^+$ T cells were further analyzed for percentage of proliferating ($Ki67^+$, in **D**), and effector ($KLRG1^+$, in **E** or $CD4^+$, in **F**) cells. These data are indicative of two independent experiments. All data are displayed as dot plots with including the median and error bars indicating interquartile range. Statistical significance was determined using the Mann–Whitney *U* test with $P < 0.05$ being statistically significant. Healthy controls were measured to depict cell frequencies and phenotypes in the non-tumor bearing host, but were not included in further statistical testing. *, $P < 0.05$; **, $P < 0.01$; ***, $P < 0.001$; ns, not significant; DC-Tx, DC therapy; Th cells, T-helper cells; Tregs, T regulatory cells.

DC therapy and combination therapy protected mice from tumor rechallenge

To investigate whether the pro-inflammatory phenotype present at day 5 following therapy persisted in treated mice, blood was extracted 3 months later (day 107) from surviving mice (treated with DC therapy, either as a monotherapy or in combination with PLX3397). At this time point, nonclassical monocyte frequencies were low but this was less pronounced as on day 15 (Fig. 6A). The percentage of PD-L1–positive nonclassical monocytes, however, was decreased and was negligible on classical monocytes (Fig. 6B). Prior to rechallenge, $CD8^+$ T-cell numbers were increased in treated mice compared with untreated tumor naïve mice, but proliferation and effector phenotype had returned to a resting state (Fig. 6C and D).

To test whether surviving CBA/J mice (Fig. 1D) were free of tumor and protected against a second tumor encounter, they were rechallenged with mesothelioma in parallel with age-matched tumor-naïve mice (Fig. 6E). Three days prior to rechallenge, PLX3397 treatment was terminated and blood was again extracted 8 days after rechallenge and recall responses were evaluated. After rechallenge, all tumor naïve mice reached their humane endpoint due to high tumor burden, whereas DC therapy-treated and combination therapy-treated mice remained disease free (Fig. 6F). $CD8^+$ T-cell numbers were higher in protected mice after challenge compared with control mice but similar in both treatment groups, whereas $CD4^+$ T-helper cells were lower in the combination therapy-treated mice (Fig. 6G). $CD8^+$ and $CD4^+$ T-cell proliferation was higher in DC+PLX3397-treated mice compared with DC-only mice, indicating superior memory responses after dual immunotherapy (Fig. 6H).

Taken together, these findings demonstrate that targeting the TME and simultaneously directing the immune system to combat cancer can lead to durable responses in mesothelioma-bearing mice and improved recall responses.

Discussion

We have shown that combination therapy using two safe anticancer treatment strategies being DC therapy and M-CSFR inhibition through the small molecule inhibitor PLX3397, results in improved overall survival and superior antitumor immune reactivity in mesothelioma mouse models. TAM-depletion in itself was insufficient to improve antitumor T-cell responses. DC-monotherapy improved survival in mice although most mice still progressed after treatment, paralleling findings in patients who develop resistance to immunotherapy (20, 21, 39). Only when PLX3397 treatment was combined with DC vaccination did we observe that the decrease in TAMs was associated with an increase in $CD8^+$ T-cell numbers and functionality, both in the TME and in the circulation. In particular, our data show that $CD8^+$ T cells, including WT1- and Mesothelin-specific $CD8^+$ T cells, in the TME of combination therapy-treated mice expressed lower

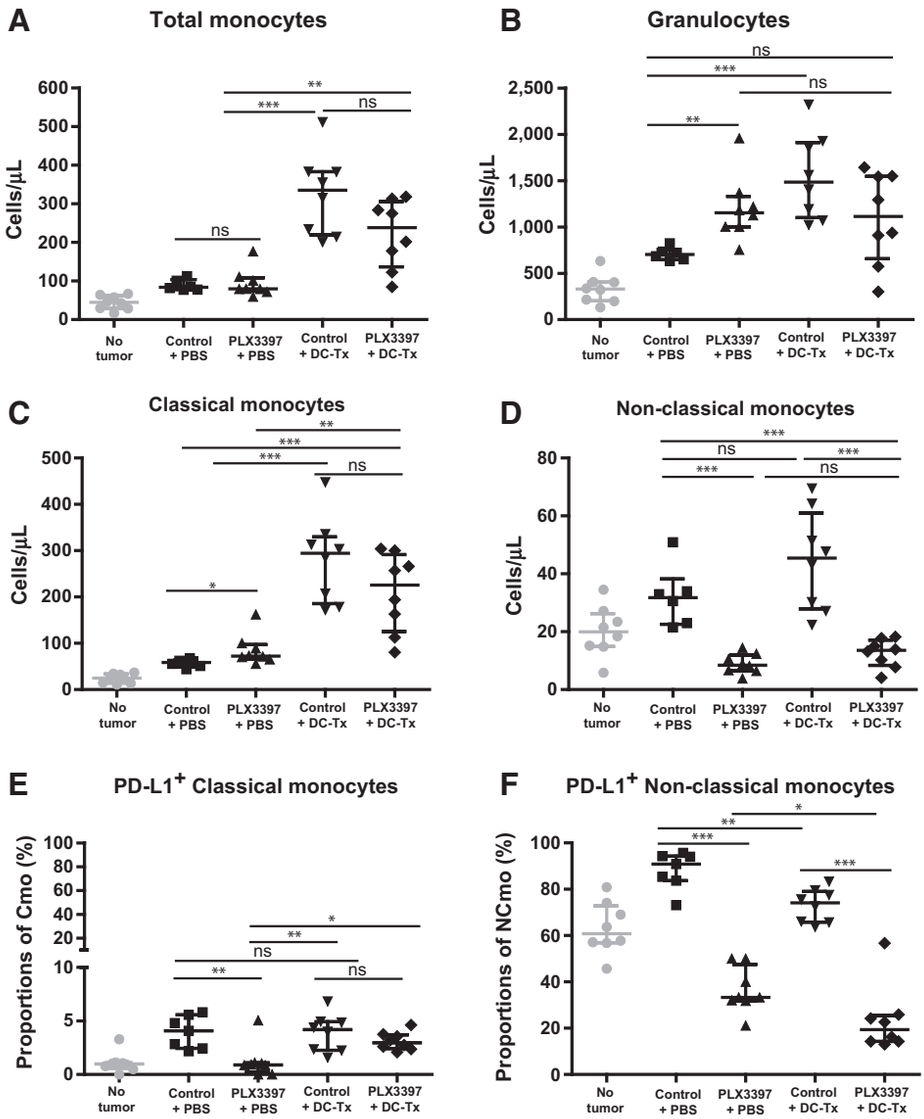

Figure 4.

Nonclassical monocytes are specifically depleted following M-CSFR inhibition and these cells are highest in PD-L1 expression in blood of mice during therapy. **A** and **B,** Total monocytes (**A**) and granulocytes (**B**) in treated tumor bearing CBA/J mice were measured in parallel with the lymphoid cell subsets depicted in Fig. 3. **C** and **D,** Monocytes were further classified into classical ($Ly6C^{high}$) and nonclassical ($Ly6C^{low/-}$) monocytes and expressed as number of cells per µL blood. **E** and **F,** PD-L1 positivity was determined on both monocyte subsets and expressed as percentage of PD-L1–positive cells in each subset. These data are indicative of two independent experiments. All data are displayed as dot plots with including the median and error bars indicating interquartile range. Statistical significance was determined using the Mann–Whitney *U* test with $P < 0.05$ being statistically significant. Healthy controls were measured to depict cell frequencies and phenotypes in the non-tumor bearing host, but were not included in further statistical testing. *, $P < 0.05$; **, $P < 0.01$; ***, $P < 0.001$; ns, not significant; DC-Tx, DC therapy; PD-L1, programmed death-ligand 1; CMo, classical monocytes; NCMo, nonclassical monocytes.

levels of key inhibitory molecules PD-1, LAG3, and TIM3, associated with exhaustion, on their cell surface. Our findings are in line with previous reports in malignant mesothelioma patients where a high ratio of $CD8^+$ T cells to M2 TAM was related to better survival (9, 12). Combining DC therapy with M-CSFR–blockade may be a safe and effective strategy to increase this clinically relevant ratio and improve disease prognosis.

TAMs are a major leukocyte subset in the stroma of mesothelioma and other cancers and capable of potently suppressing endogenous or treatment-induced antitumor T-cell responses (8, 11). Depletion of this immune suppressive cell type may, thus, render previously immune resistant or escaped tumors sensitive to checkpoint inhibition (40), chemo- and radiotherapy (41, 42), and cellular therapies such as adoptive T-cell transfer (43) and now also DC therapy. Use of chemo(radio)therapy or PD-1 checkpoint inhibitors either come with burdensome side effects or are most effective in boosting a preexisting antitumor T-cell response (3, 4). DC therapy effectively induces novel antitumor immune responses which can then be sustained by targeting the generally immune suppressive TME (23, 44).

M-CSFR inhibition depletes TAMs in multiple tumor models but its effects on survival as monotherapy or combined with other therapies are variable (16, 18, 41, 45). For example, when M-CSFR inhibition was combined with a tumor vaccine or with certain chemotherapeutic drugs, efficacy of these therapies was abrogated, questioning the role of TAMs in tumor behavior and response to these therapies (16, 45, 46). On the other hand, glioblastoma (GBM)-bearing mice treated with the M-CSFR–inhibitor BLZ945 as monotherapy showed improved survival (16). Although resistance to monotherapy ensued in the majority of mice, tumors regressed due to skewing of M2 to M1 TAMs rather than TAM depletion. In our models, M-CSFR inhibitor monotherapy alone did not prolong survival despite gross changes in stromal composition. These differences in drug efficacy may be explained by TAM-dependency of certain therapies, mechanism of M-CSFR inhibition, or timing of therapy and tumor stage and type

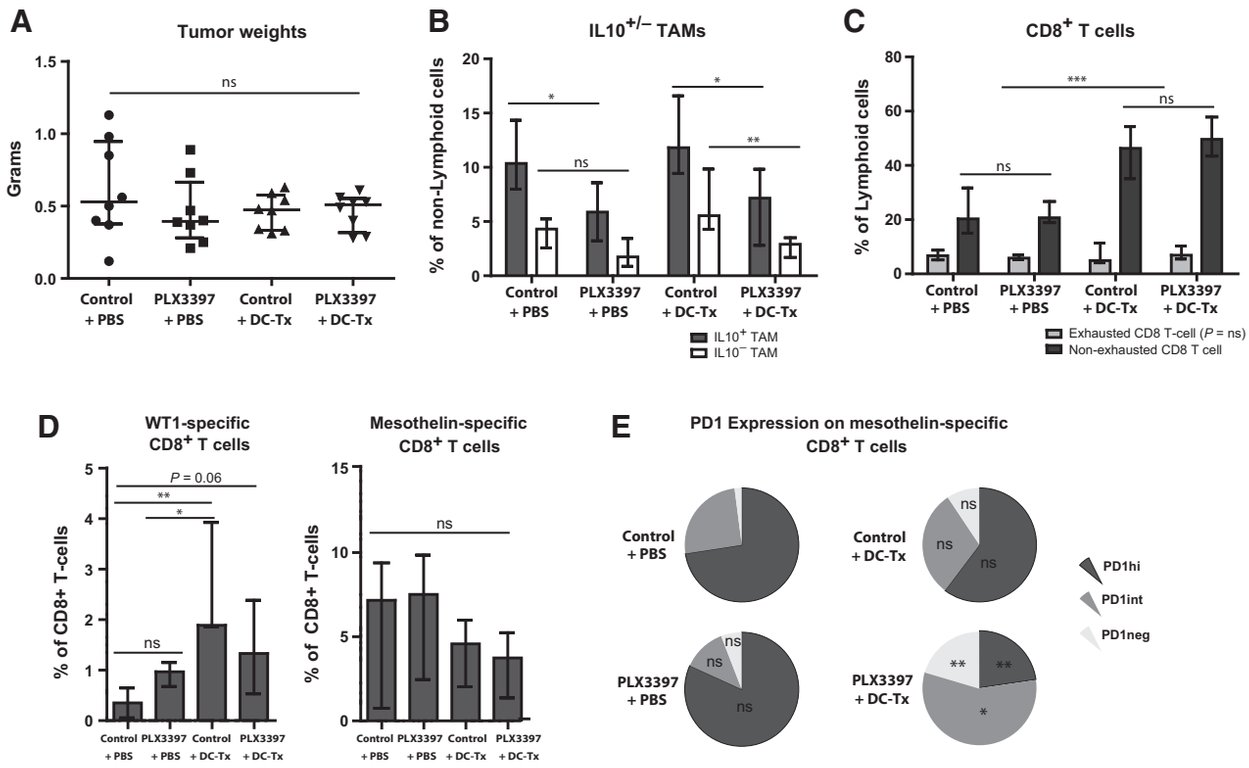

Figure 5.

M-CSFR inhibition decreases tumor-associated macrophages in mesothelioma and improves the DC therapy induced $CD8^+$ T-cell phenotype. Identical to previous experiments, CBA/J mice were intraperitoneally inoculated with tumor cells and treated on day 10 with either DC therapy or control PBS, and/or continuous PLX3397- or control treatment. Only now, mice were sacrificed on $t = 15$ days to examine the TME, blood and spleen in the different treatment groups. For **D-E**, mice were treated at day 15 with either PLX3397 and/or DC therapy and sacrificed 8 days later when tumors were harvested and analyzed. **A,** Tumors were extracted from the peritoneal cavity and weighed. **B,** Tumors were dissociated and single-cell suspensions that were stained and analyzed by flow cytometry. TAMs were divided into IL10-positive and -negative and denoted as percentage of non-lymphoid cells, to correct for changes in lymphoid cells due to treatment. **C,** Similar to **B**, $CD8^+$ TILs) were identified. The distinction was made between "exhausted" [Program Death 1^+ (PD-1), Lymphocyte-activating-gene 3^+, ($LAG3^+$) and Interferonγ (IFNγ] and "non-exhausted" ($PD\text{-}1^-$, $LAG3^-$, and $IFN\gamma^+$) $CD8^+$ TILs. Cells were depicted as percentage of total lymphoid cells, to correct for changes in the myeloid compartment due to treatment. **D,** The frequencies of WT-1 and Mesothelin-specific T cells were determined in the tumors of mice treated with or without PLX3397 and/or DC therapy using dextramers. **E,** Pie charts depicting the distribution of PD-1 expression on Mesothelin-specific $CD8^+$ T cells in the tumors of mice untreated or treated with the different immunotherapies as monotherapy, or in combination. All data are displayed as dot plots or bar graphs including the median and error bars indicating interquartile range. Pie charts are used to display distribution of PD-1 expression on $CD8^+$ T cells in the different treatment arms. Statistical significance was determined using the Mann–Whitney *U* test with $P < 0.05$ being statistically significant. *, $P < 0.05$; **, $P < 0.01$; ***, $P < 0.001$; ns, not significant; DC-Tx, DC therapy; TAM, tumor-associated macrophage; IL10, Interleukin 10, WT1, Wilms Tumor 1; PD-1, programmed cell death protein 1; PD-1hi, PD-1-high; PD-1int, PD-1-intermediate; PD-1neg; PD-1-negative.

(46). In the GBM model, for example, TAM skewing was dependent on glioblastoma cell-derived factors including granulocyte-macrophage colony stimulating factor (GM-CSF) (16). GM-CSF is often used to culture pro-inflammatory M1 macrophages and DCs whereas M-CSF cultured macrophages display a M2 phenotype (14, 28, 47). Other tumor types such as mesothelioma, both in patient and in mice, produce considerable amounts of M-CSF but much less GM-CSF (Supplementary Fig. S1; ref. 48), providing a likely explanation for the depletion rather than skewing of TAMs in our models.

Although $CD8^+$ TILs were present in mesothelioma tumors of untreated mice, they did not increase in frequency or functionality following TAM-depletion and maintained an exhausted, dysfunctional phenotype. After induction of an immune response using DC therapy in late stage disease, functional TIL frequencies increased. Survival was unaltered in BALB/c mice, and, although prolonged in the CBA/J model, those mice showed disease progression or recurrence during follow-up. Tumor responses were only durable in the majority of mice when DC therapy was applied in a TAM-deficient TME. We could detect this synergy between therapies in T-cell proliferation and phenotype in blood during therapy and after rechallenge, and in the tumor where T-cell phenotype was improved following TAM depletion. Which immune suppressive property of TAMs is key to induction of T-cell exhaustion in our model remains to be full elucidated, but most likely involves multiple factors (e.g., IL10, arginase, PD-L1; ref. 8, 49).

Uncertainty remains about the ontogeny of TAMs in solid tumors. We appreciate that classical (Ly6Chi) monocytes are the main precursors of inflammatory DCs and macrophages including TAMs, but note incongruence regarding the sequence of events that precede M2-TAM development (50, 51). Classical monocytes

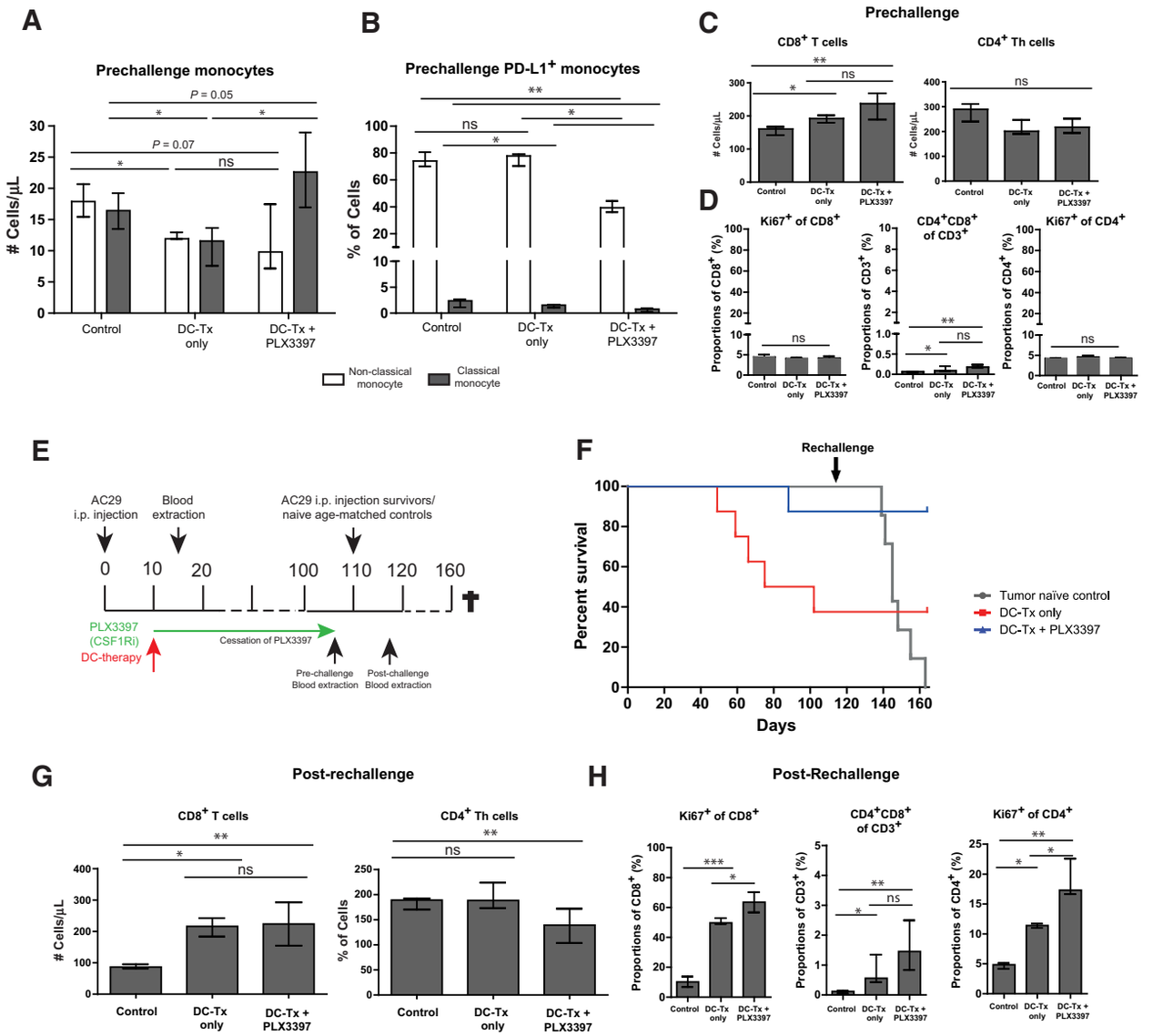

Figure 6.

Mice treated with DC therapy and/or M-CSFR inhibition were protected from tumor rechallenge with combination therapy-treated mice displaying superior recall responses. **A** and **B,** Monocyte subsets and related PD-L1 expression was assessed by flow cytometry in blood prior to rechallenge. **C** and **D,** $CD8^+$ and $CD4^+$ T-cell frequencies and proliferation status as determined by Ki-67 were evaluated using flow cytometry. **E,** Surviving mice from the experiment described in Fig. 1 and age-matched tumor naïve mice were rechallenged and subsequently monitored for signs of illness. Three days prior to rechallenge, PLX3397-treatment in the combination therapy-treated mice was terminated and mice were put on control chow for the further duration of the experiment. Also, blood was extracted at that time point, and again 8 days after rechallenge. **F,** Kaplan–Meier curve of survival following rechallenge. For DC-only (red) and combination therapy-treated mice (blue), curves were identical to the KM-curve in Fig. 1 but on day $t = 110$, mice were rechallenged. Tumor naïve littermates (*gray*) were injected with tumor cells in parallel to ensure tumor pathogenicity and correct for age. **G** and **H,** T-cell features as in **C** and **D** were analyzed in DC-only, DC+PLX3397 combination and untreated mice before and after rechallenge. All data are displayed as bar graph or line graphs including the median and error bars indicating interquartile range. Statistical significance was determined using the Mann–Whitney *U* test with $P < 0.05$ being statistically significant. *, $P < 0.05$; **, $P < 0.01$; ***, $P < 0.001$; ns, not significant; DC-Tx, DC therapy; PD-L1, programmed death-ligand 1.

are obligatory precursors of nonclassical monocytes; the functions and migration patterns of both cell types differ, with nonclassical monocytes being crucial for endothelial and tissue integrity (32, 33). Nonclassical monocytes are particularly dependent on M-CSF for their survival (13, 52). Nonclassical monocytes and TAMs share a similar immune suppressive phenotype and are most sensitive to M-CSFR inhibition, suggesting a relationship between these cell types. Future research will have to further delineate the contribution of nonclassical monocytes to TAMs in cancer.

In conclusion, we have demonstrated that therapeutic efficacy of M-CSFR inhibition as monotherapy is limited in mesothelioma. However, TAM depletion combined with an effective DC-

mediated antitumor T-cell response is capable of producing durable tumor responses and functional antitumor immunity.

Disclosure of Potential Conflicts of Interest

J.G. Aerts reports receiving commercial research grant from Amphera, has ownership interest (including patents) in dendritic cell immunotherapy with an allogenic lysate, and is a consultant/advisory board member for AstraZeneca, Bristol-Myers Squibb, Boehringer Ingelheim, Eli Lilly and Company, MSD, and Roche. No potential conflicts of interest were disclosed by the other authors.

Authors' Contributions

Conception and design: F. Dammeijer, L.A. Lievense, K. Bezemer, R.W. Hendriks, J.G. Aerts
Development of methodology: F. Dammeijer, L.A. Lievense, K. Bezemer, J.P. Hegmans, J.G. Aerts
Acquisition of data (provided animals, acquired and managed patients, provided facilities, etc.): F. Dammeijer, L.A. Lievense, J.G. Aerts
Analysis and interpretation of data (e.g., statistical analysis, biostatistics, computational analysis): F. Dammeijer, L.A. Lievense, J.G. Aerts
Writing, review, and/or revision of the manuscript: F. Dammeijer, L.A. Lievense, T. van Hall, R.W. Hendriks, J.G. Aerts
Administrative, technical, or material support (i.e., reporting or organizing data, constructing databases): F. Dammeijer, M.E. Kaijen-Lambers, M. van Nimwegen, K. Bezemer, J.P. Hegmans
Study supervision: R.W. Hendriks, J.G. Aerts

Acknowledgments

The authors would like to acknowledge Plexxikon for distributing to us PLX3397 as part of a material transfer agreement. We thank R. Bouzid and the Erasmus MC Animal Facility staff for their support with the animal experiments.

The costs of publication of this article were defrayed in part by the payment of page charges. This article must therefore be hereby marked *advertisement* in accordance with 18 U.S.C. Section 1734 solely to indicate this fact.

Received November 4, 2016; revised March 30, 2017; accepted May 16, 2017; published OnlineFirst May 23, 2017.

References

1. Postow MA, Callahan MK, Wolchok JD. Immune checkpoint blockade in cancer therapy. J Clin Oncol 2015;33:1974–82.
2. Gajewski TF. The next hurdle in cancer immunotherapy: overcoming the non-T-cell-inflamed tumor microenvironment. Semin Oncol 2015;42: 663–71.
3. Smyth MJ, Ngiow SF, Ribas A, Teng MW. Combination cancer immunotherapies tailored to the tumour microenvironment. Nat Rev Clin Oncol 2016;13:143–58.
4. Teng MW, Ngiow SF, Ribas A, Smyth MJ. Classifying cancers based on T-cell infiltration and PD-L1. Cancer Res 2015;75:2139–45.
5. Tumeh PC, Harview CL, Yearley JH, Shintaku IP, Taylor EJ, Robert L, et al. PD-1 blockade induces responses by inhibiting adaptive immune resistance. Nature 2014;515:568–71.
6. Taioli E, Wolf AS, Camacho-Rivera M, Kaufman A, Lee DS, Nicastri D, et al. Determinants of survival in malignant pleural mesothelioma: a surveillance, epidemiology, and end results (SEER) study of 14,228 patients. PloS One 2015;10:e0145039.
7. Lievense LA, Bezemer K, Aerts JG, Hegmans JP. Tumor-associated macrophages in thoracic malignancies. Lung Cancer 2013;80: 256–62.
8. Noy R, Pollard JW. Tumor-associated macrophages: from mechanisms to therapy. Immunity 2014;41:49–61.
9. Cornelissen R, Lievense LA, Maat AP, Hendriks RW, Hoogsteden HC, Bogers AJ, et al. Ratio of intratumoral macrophage phenotypes is a prognostic factor in epithelioid malignant pleural mesothelioma. PloS One 2014;9:e106742.
10. Cornelissen R, Lievense LA, Robertus JL, Hendriks RW, Hoogsteden HC, Hegmans JP, et al. Intratumoral macrophage phenotype and CD8 T lymphocytes as potential tools to predict local tumor outgrowth at the intervention site in malignant pleural mesothelioma. Lung Cancer 2015;88:332–7.
11. Lievense LA, Cornelissen R, Bezemer K, Kaijen-Lambers ME, Hegmans JP, Aerts JG. Pleural effusion of patients with malignant mesothelioma induces macrophage-mediated T cell suppression. J Thorac Oncol 2016;11:1755–64.
12. Ujiie H, Kadota K, Nitadori JI, Aerts JG, Woo KM, Sima CS, et al. The tumoral and stromal immune microenvironment in malignant pleural mesothelioma: a comprehensive analysis reveals prognostic immune markers. Oncoimmunology 2015;4:e1009285.
13. Hume DA, MacDonald KP. Therapeutic applications of macrophage colony-stimulating factor-1 (CSF-1) and antagonists of CSF-1 receptor (CSF-1R) signaling. Blood 2012;119:1810–20.
14. Van Overmeire E, Stijlemans B, Heymann F, Keirsse J, Morias Y, Elkrim Y, et al. M-CSF and GM-CSF receptor signaling differentially regulate monocyte maturation and macrophage polarization in the tumor microenvironment. Cancer Res 2016;76:35–42.
15. Laoui D, Van Overmeire E, De Baetselier P, Van Ginderachter JA, Raes G. Functional relationship between tumor-associated macrophages and macrophage colony-stimulating factor as contributors to cancer progression. Front Immunol 2014;5:489.
16. Pyonteck SM, Akkari L, Schuhmacher AJ, Bowman RL, Sevenich L, Quail DF, et al. CSF-1R inhibition alters macrophage polarization and blocks glioma progression. Nat Med 2013;19:1264–72.
17. Tap WD, Wainberg ZA, Anthony SP, Ibrahim PN, Zhang C, Healey JH, et al. Structure-guided blockade of CSF1R kinase in tenosynovial giant-cell tumor. N Engl J Med 2015;373:428–37.
18. Butowski N, Colman H, De Groot JF, Omuro AM, Nayak L, Wen PY, et al. Orally administered colony stimulating factor 1 receptor inhibitor PLX3397 in recurrent glioblastoma: an ivy foundation early phase clinical trials consortium phase II study. Neuro Oncol 2016; 18:557–64.
19. Dammeijer F, Lievense LA, Veerman GD, Hoogsteden HC, Hegmans JP, Arends LR, et al. The efficacy of tumor vaccines and cellular immunotherapies in non-small cell lung cancer: a systematic review and meta-analysis. J Clin Oncol 2016;34:3204–12.
20. Hegmans JP, Veltman JD, Lambers ME, de Vries IJ, Figdor CG, Hendriks RW, et al. Consolidative dendritic cell-based immunotherapy elicits cytotoxicity against malignant mesothelioma. Am J Respir Crit Care Med 2010;181:1383–90.
21. Cornelissen R, Hegmans JP, Maat AP, Kaijen-Lambers ME, Bezemer K, Hendriks RW, et al. Extended tumor control after dendritic cell vaccination with low dose cyclophosphamide as adjuvant treatment in patients with malignant pleural mesothelioma. Am J Respir Crit Care Med 2015;193: 1023–31.
22. Davis MR, Manning LS, Whitaker D, Garlepp MJ, Robinson BW. Establishment of a murine model of malignant mesothelioma. Int J Cancer 1992;52:881–6.
23. Hegmans JP, Hemmes A, Aerts JG, Hoogsteden HC, Lambrecht BN. Immunotherapy of murine malignant mesothelioma using tumor lysate-pulsed dendritic cells. Am J Respir Crit Care Med 2005;171: 1168–77.
24. Sluijter M, van der Sluis TC, van der Velden PA, Versluis M, West BL, van der Burg SH, et al. Inhibition of CSF-1R supports T-cell mediated melanoma therapy. PLoS One 2014;9:e104230.
25. Veltman JD, Lambers ME, van Nimwegen M, de Jong S, Hendriks RW, Hoogsteden HC, et al. Low-dose cyclophosphamide synergizes with dendritic cell-based immunotherapy in antitumor activity. J Biomed Biotechnol 2010;2010:798467.
26. Veltman JD, Lambers ME, van Nimwegen M, Hendriks RW, Hoogsteden HC, Hegmans JP, et al. Zoledronic acid impairs myeloid differentiation to tumour-associated macrophages in mesothelioma. Br J Cancer 2010;103: 629–41.

27. Robinson BW, Lake RA. Advances in malignant mesothelioma. N Engl J Med 2005;353:1591–603.
28. Helft J, Bottcher J, Chakravarty P, Zelenay S, Huotari J, Schraml BU, et al. GM-CSF mouse bone marrow cultures comprise a heterogeneous population of CD11c(+)MHCII(+) macrophages and dendritic cells. Immunity 2015;42:1197–211.
29. Moughon DL, He H, Schokrpur S, Jiang ZK, Yaqoob M, David J, et al. Macrophage blockade using CSF1R inhibitors reverses the vascular leakage underlying malignant ascites in late-stage epithelial ovarian cancer. Cancer Res 2015;75:4742–52.
30. Kitchen SG, Jones NR, LaForge S, Whitmire JK, Vu BA, Galic Z, et al. CD4 on CD8(+) T cells directly enhances effector function and is a target for HIV infection. Proc Natl Acad Sci U S A 2004;101:8727–32.
31. Olson JA, McDonald-Hyman C, Jameson SC, Hamilton SE. Effector-like CD8(+) T cells in the memory population mediate potent protective immunity. Immunity 2013;38:1250–60.
32. Geissmann F, Jung S, Littman DR. Blood monocytes consist of two principal subsets with distinct migratory properties. Immunity 2003; 19:71–82.
33. Yona S, Kim KW, Wolf Y, Mildner A, Varol D, Breker M, et al. Fate mapping reveals origins and dynamics of monocytes and tissue macrophages under homeostasis. Immunity 2013;38:79–91.
34. Wherry EJ. T cell exhaustion. Nat Immunol 2011;12:492–9.
35. Ngiow SF, Young A, Jacquelot N, Yamazaki T, Enot D, Zitvogel L, et al. A threshold level of intratumor CD8+ T-cell PD-1 expression dictates therapeutic response to anti-PD-1. Cancer Res 2015;75:3800–11.
36. Im SJ, Hashimoto M, Gerner MY, Lee J, Kissick HT, Burger MC, et al. Defining CD8+ T cells that provide the proliferative burst after PD-1 therapy. Nature 2016;537:417–21.
37. Chen DS, Mellman I. Elements of cancer immunity and the cancer-immune set point. Nature 2017;541:321–30.
38. Gros A, Robbins PF, Yao X, Li YF, Turcotte S, Tran E, et al. PD-1 identifies the patient-specific CD8(+) tumor-reactive repertoire infiltrating human tumors. J Clin Invest 2014;124:2246–59.
39. Kelderman S, Schumacher TN, Haanen JB. Acquired and intrinsic resistance in cancer immunotherapy. Mol Oncol 2014;8:1132–9.
40. Zhu Y, Knolhoff BL, Meyer MA, Nywening TM, West BL, Luo J, et al. CSF1/CSF1R blockade reprograms tumor-infiltrating macrophages and improves response to T-cell checkpoint immunotherapy in pancreatic cancer models. Cancer Res 2014;74:5057–69.
41. DeNardo DG, Brennan DJ, Rexhepaj E, Ruffell B, Shiao SL, Madden SF, et al. Leukocyte complexity predicts breast cancer survival and functionally regulates response to chemotherapy. Cancer Discov 2011; 1:54–67.
42. Xu J, Escamilla J, Mok S, David J, Priceman S, West B, et al. CSF1R signaling blockade stanches tumor-infiltrating myeloid cells and improves the efficacy of radiotherapy in prostate cancer. Cancer Res 2013;73:2782–94.
43. Mok S, Koya RC, Tsui C, Xu J, Robert L, Wu L, et al. Inhibition of CSF-1 receptor improves the antitumor efficacy of adoptive cell transfer immunotherapy. Cancer Res 2014;74:153–61.
44. Carreno BM, Magrini V, Becker-Hapak M, Kaabinejadian S, Hundal J, Petti AA, et al. A dendritic cell vaccine increases the breadth and diversity of melanoma neoantigen-specific T cells. Science 2015;348:803–8.
45. van der Sluis TC, Sluijter M, van Duikeren S, West BL, Melief CJ, Arens R, et al. Therapeutic peptide vaccine-induced CD8 T cells strongly modulate intratumoral macrophages required for tumor regression. Cancer Immunol Res 2015;3:1042–51.
46. De Palma M, Lewis CE. Macrophage regulation of tumor responses to anticancer therapies. Cancer Cell 2013;23:277–86.
47. Lacey DC, Achuthan A, Fleetwood AJ, Dinh H, Roiniotis J, Scholz GM, et al. Defining GM-CSF- and macrophage-CSF-dependent macrophage responses by in vitro models. J Immunol 2012;188:5752–65.
48. Chene AL, d'Almeida S, Blondy T, Tabiasco J, Deshayes S, Fonteneau JF, et al. Pleural effusions from mesothelioma patients induce recruitment of monocytes and their differentiation into M2 macrophages. J Thorac Oncol 2016;11:1765–73.
49. Joyce JA, Fearon DT. T cell exclusion, immune privilege, and the tumor microenvironment. Science 2015;348:74–80.
50. Franklin RA, Liao W, Sarkar A, Kim MV, Bivona MR, Liu K, et al. The cellular and molecular origin of tumor-associated macrophages. Science 2014; 344:921–5.
51. Movahedi K, Laoui D, Gysemans C, Baeten M, Stange G, Van den Bossche J, et al. Different tumor microenvironments contain functionally distinct subsets of macrophages derived from Ly6C(high) monocytes. Cancer Res 2010;70:5728–39.
52. MacDonald KP, Palmer JS, Cronau S, Seppanen E, Olver S, Raffelt NC, et al. An antibody against the colony-stimulating factor 1 receptor depletes the resident subset of monocytes and tissue- and tumor-associated macrophages but does not inhibit inflammation. Blood 2010;116:3955–63.